Solution Structure and NH Exchange Studies of the MutT Pyrophosphohydrolase Complexed with Mg^{2+} and 8-Oxo-dGMP, a Tightly Bound Product[†,‡]

Michael A. Massiah, Vibhor Saraswat, Hugo F. Azurmendi, and Albert S. Mildvan*

Department of Biological Chemistry, The Johns Hopkins School of Medicine, 725 North Wolfe Street, Baltimore, Maryland 21205-2185

Received April 25, 2003; Revised Manuscript Received June 18, 2003

ABSTRACT: To learn the structural basis for the unusually tight binding of 8-oxo-nucleotides to the MutT pyrophosphohydrolase of *Escherichia coli* (129 residues), the solution structure of the MutT-Mg^{2+}-8-oxo-dGMP product complex ($K_D = 52$ nM) was determined by standard 3-D heteronuclear NMR methods. Using 1746 NOEs (13.5 NOEs/residue) and 186 ϕ and ψ values derived from backbone ^{15}N, Cα, Hα, and Cβ chemical shifts, 20 converged structures were computed with NOE violations $\leq$0.25 Å and total energies $\leq$450 kcal/mol. The pairwise root-mean-square deviations (RMSD) of backbone N, Cα, and C′ atoms for the secondary structured regions and for all residues of the 20 structures are 0.65 and 0.98 Å, respectively, indicating a well-defined structure. Further refinement using residual dipolar coupling from 53 backbone N−H vectors slightly improved the RMSD values to 0.49 and 0.84 Å, respectively. The secondary structures, which consisted of two α-helices and a five-stranded mixed β-sheet, were indistinguishable from those of free MutT and of MutT in the quaternary MutT-Mg^{2+}-(H_2O)-AMPCPP-Mg^{2+} complex. Comparisons of these three tertiary structures showed a narrowing of the hydrophobic nucleotide-binding cleft in the 8-oxo-dGMP complex resulting from a 2.5−4.5 Å movement of helix I and a 1.5 Å movement of helix II and loop 4 toward the cleft. The binding of 8-oxo-dGMP to MutT-Mg^{2+} buries 71−78% of the surface area of the nucleotide. The $10^{3.7}$-fold weaker binding substrate analogue Mg^{2+}-AMPCPP induced much smaller changes in tertiary structure, and MutT buried only 57% of the surface of the AMP moiety of AMPCPP. Formation of the MutT-Mg^{2+}-8-oxo-dGMP complex slowed the backbone NH exchange rates of 45 residues of the enzyme by factors of 10^1−10^6 as compared with the MutT-Mg^{2+} and the MutT-Mg^{2+}-dGMP complexes, suggesting a more compact structure when 8-oxo-dGMP is bound. The $10^{4.6}$-fold weaker binding of dGMP to MutT-Mg^{2+} ($K_D = 1.8$ mM) slowed the backbone exchange rates of only 20 residues and by smaller factors of ~10. Hence, the high affinity of MutT-Mg^{2+} for 8-oxo-dGMP likely results from widespread ligand-induced conformation changes that narrow the nucleotide binding site and lower the overall free energy of the enzyme−product complex. Specific hydrogen bonding of the purine ring of 8-oxo-dGMP by the side chains of Asn-119 and Arg-78 may also contribute.

The MutT enzyme from *Escherichia coli* (129 residues) is a prototypical Nudix hydrolase[1] that catalyzes the hydrolysis of nucleoside and deoxynucleoside triphosphates (NTP) by substitution at the rarely attacked β-phosphorus to yield a nucleotide (NMP) and inorganic pyrophosphate (PPi) (eq 1) (*1*−*3*).

$$NTP + H_2O \rightarrow NMP + PPi + H^+ \qquad (1)$$

The enzyme requires two divalent cations for activity, one coordinated to the β- and γ-phosphoryl groups of the NTP substrate and the other coordinated to the enzyme (*4*). Product inhibition and product binding studies (*5*) indicate a uni-bi-iso kinetic mechanism, with PPi dissociating from the product complex first, followed by the nucleotide, leaving an altered form of the enzyme, which slowly reverts to the form that binds substrate. A chemical mechanism for MutT has been proposed (*5*), consistent with the solution structure of the MutT-Mg^{2+}-(H_2O)-AMPCPP-Mg^{2+} complex (*6*), and with mutagenesis studies (*7*), in which Glu-53 is displaced from the enzyme-bound Mg^{2+} by Glu-98 in the slow iso step, thereby permitting the binding of the NTP substrate and the subsequent deprotonation of the attacking water by Glu-53.

The biological role of the MutT enzyme is to prevent errors in DNA replication by hydrolyzing mutagenic nucleotides

[†] This research was supported by National Institutes of Health Grant DK28616 (to A.S.M.).

[‡] Complete listings of the distance restraints derived from NOE data, chemical shifts, and dipolar couplings have been deposited in the Protein Data Bank (PDB) together with the atomic coordinates of the families of 20 acceptable structures (case 1, file name 1PPX; case 2, 1PUN; case 3, 1PUQ; and case 4, 1PUS). The chemical shifts have been deposited in the BioMagResBank (BMRB, entry number 5866).

* To whom correspondence should be addressed. Phone: (410) 955-2038. Fax: (410) 955-5759. E-mail: mildvan@welchlink.welch.jhu.edu.

[1] Abbreviations: 8-oxo-dGMP, 8-oxo-deoxyguanosine monophosphate; HSQC, heteronuclear single quantum coherence; NOESY, nuclear Overhauser effect spectroscopy; NMP, nucleoside monophosphate; NTP, nucleoside triphosphate; Nudix hydrolase, nucleoside diphosphate-X hydrolase; PPi, pyrophosphate; TOCSY, total correlation spectroscopy.

10.1021/bi030105p CCC: $25.00
Published on Web 08/07/2003

such as 8-oxo-dGTP (*8*), a product of oxidative damage to guanine nucleotides, which can mispair with template adenine during DNA replication (*9*, *10*). Accordingly, MutT-deficient *E. coli* show a 10^4-fold increase in mutations, all of which are AT → CG transversions (*11*, *12*), and inactivation of a homologous 8-oxo-dGTPase in mice results in major increases in the occurrence of tumors (*13*). Although the actual in vivo substrate of the MutT enzyme has not been rigorously identified (*14*), 8-oxo-dGTP is the best substrate in vitro, with a K_m that is $10^{3.4}$-fold lower (0.48 μM) than that of dGTP (1100 μM) but with the same k_{cat} (4 s^{-1}) (*8*).

Extremely high affinity of MutT for an 8-oxo-nucleotide was established by studies of the reaction product 8-oxo-dGMP, which was found to bind to one site on the Mg^{2+} enzyme with a K_D (52 nM) that is $10^{4.6}$-fold lower than that of dGMP (1.8 mM) (5). The unusually tight binding of 8-oxo-dGMP ($\Delta G° = -9.8$ kcal/mol) is driven by a favorable enthalpy change ($\Delta H = -32$ kcal/mol), exceeding an unfavorable entropy change ($-T\Delta S° = +22$ kcal/mol), the latter indicating a strong ordering of the MutT-Mg^{2+}-8-oxo-dGMP complex (*5*). In the solution structure of the MutT-Mg^{2+}-(H_2O)-AMPCPP-Mg^{2+} complex, the AMP moiety of enzyme-bound AMPCPP directly contacts only five residues of MutT, and nine additional residues form a second shell (*5*, *6*). However, the binding of 8-oxo-dGMP to a single site on the enzyme−Mg^{2+} complex altered the backbone ^{15}N and/or NH chemical shifts of 62 residues widely distributed throughout the protein, indicating diffuse structural changes throughout the protein (*5*).

Comparison of the solution structure of the weak, quaternary MutT-Mg^{2+}-(H_2O)-AMPCPP-Mg^{2+} complex (*6*) with that of free MutT (*15*) revealed identical secondary structures of the protein and only small differences in tertiary structure. To elucidate the structural basis for the unusually tight binding of 8-oxo-dGMP, we have determined the solution structure of the MutT-Mg^{2+}-8-oxo-dGMP complex and have measured the backbone NH exchange rates of this and other complexes of MutT. A preliminary abstract of this work has been published (*16*).

EXPERIMENTAL PROCEDURES

Materials. Isopropyl β-D-thiogalactoside (IPTG) was from Roche (Indianapolis, IN). Tryptone and yeast extract were obtained from Difco (Detroit, MI). Ammonium sulfate, ampicillin, 2′-deoxyguanosine-5′-monophosphate, 2′-deoxyguanosine-5′-triphosphate, 1-octanol, pentaethylene glycol monooctyl ether (C8E5), dithiothreitol (DTT), lysozyme, and streptomycin sulfate were from Sigma (St. Louis, MO). Vivaspin (MWCO 5000) centrifugal concentrators were purchased from Vivascience Limited (Gloucestershire, UK). Sephadex G-100 and DEAE-Sepharose fast-flow were from Pharmacia Biotech (Piscataway, NJ). Deuterium oxide (D_2O 99.96% D) was from Aldrich (Milwaukee, WI). Uniformly (99%) ^{15}N-enriched $^{15}NH_4Cl$ and uniformly (99%) ^{13}C-enriched D-glucose were from Isotech Inc. (Miamisburg, OH). All solvents and reagents were of the highest purity available, and buffers were treated with Chelex-100 before use to remove trace metals.

Preparation of MutT and 8-Oxo-dGMP. The recombinant *E. coli* strain HMS174(DE3)[pETMutT] was used for the production of unlabeled, uniformly ^{15}N-labeled, and uniformly ^{13}C- and ^{15}N-labeled protein (*17*). The enzyme was purified to >95% homogeneity on the basis of SDS−PAGE and specific activity (500 IU/mg) and was concentrated for NMR studies as described (*5*, *7*). The synthesis, purification, and characterization of 8-oxo-dGMP were carried out as previously described (*5*). Residual tetraethylammonium-bicarbonate was removed by reverse phase HPLC using a C_{18}-Aqua column (Phenomenex, Torrance, CA).

NMR Spectroscopy. All NMR data were collected at 23 °C on a Varian UnityPlus 600 MHz NMR spectrometer equipped with a pulse field gradient unit and a Varian 5 mm triple resonance actively shielded *z*-gradient probe. The data were recorded using States-TPPI in all indirect dimensions. NMR samples typically contained 1 mM MutT, 15 mM $MgCl_2$, 4 mM d_{11}-Tris-HCl, pH 7.5, 21 mM NaCl, 0.34 mM NaN_3, and 10% D_2O. Because 8-oxo-dGMP binds tightly to MutT (K_D = 52 nM) (*5*), the MutT-Mg^{2+}-8-oxo-dGMP samples also contained 1.3 mM 8-oxo-dGMP. Since dGMP binds weakly to MutT (K_D = 1.8 mM) (*5*), the MutT-Mg^{2+}-dGMP samples contained 20 mM dGMP and a total of 35 mM $MgCl_2$, to maintain constancy of the concentration of free Mg^{2+}.

The orienting medium used for measurements of residual dipolar couplings was a 3% (w/v) bicelle solution of pentaethylene glycol monooctyl ether to which was added 1-octanol at a molar ratio of [ether]/[octanol] of 0.87 (*18*). This medium induced a 17.3 Hz quadrupolar splitting of the ^2H signal of D_2O.

The ^1H-^{15}N HSQC spectrum of the MutT-Mg^{2+}-8-oxo-dGMP complex was very different from those of free MutT (*17*), the MutT-Mg^{2+}-dGMP complex (*5*), and the MutT-Mg^{2+}-(H_2O)-AMPCPP-Mg^{2+} complex (*6*). Hence, reassignment of the protein backbone and side-chain ^1H, ^{15}N, and ^{13}C resonances was essential. Assignments were obtained using the 3-D HNCA, 3-D HNCACB, 2-D ^1H-^1H NOESY, 2-D ^1H-^1H TOCSY, 3-D ^1H-^{15}N NOESY-HSQC, and 3-D ^1H-^{15}N TOCSY-HSQC spectra. The HNCA and HNCACB data, in most cases, revealed stronger intra- than interresidue signals, clearly making this distinction. These data were also correlated with Hα-$NH_{(i,i+1)}$ and NH-$NH_{(i,i+1)}$ NOEs, confirming the Cα and Cβ assignments.

Tertiary structural information was obtained from the 3-D ^1H-^{13}C NOESY-HSQC spectrum as well as from the 2-D ^1H-^1H NOESY and 3-D ^1H-^{15}N NOESY HSQC spectra. The NOESY and TOCSY data were collected with a mixing time of 150 ms and a spinlock of 65 ms, respectively. The residual dipolar couplings of backbone ^{15}N-H groups were determined as described (*19*), from in phase/anti phase ^1H-^{15}N HSQC spectra, with and without orienting bicelles (*18*). The data were processed with nmrPipe (*20*) and analyzed with NMRview (*21*).

To define the binding site of 8-oxo-dGMP, a 3-D ^{13}C/^{12}C-edited-NOE-filtered experiment was performed as described (*22*, *23*). Because 8-oxo-dGMP binds tightly to MutT (K_D = 52 nM) (*5*), the sample contained 0.5 mM ^{15}N/^{13}C-labeled enzyme and 0.6 mM unlabeled 8-oxo-dGMP in the presence of 15 mM $MgCl_2$, 4 mM d_{11}-Tris-HCl, pH 7.5 (in H_2O), 21 mM NaCl, 0.34 mM NaN_3, and 99.9% D_2O. In addition, a 2-D ^1H-^1H NOESY spectrum with a mixing time of 800 ms and a dqf-COSY spectrum of free 0.4 mM 8-oxo-dGMP in 99.9% D_2O (pH 7.5 in H_2O) were collected to assign the nonexchangeable protons of the deoxyribose ring.

Table 1: Sets of Restraints Involving 8-Oxo-dGMP Used in Computing the Structure of the MutT-Mg^{2+}-8-oxo-dGMP Complex

	nucleotide conformation	nucleotide orientation	other
case 1	same as bound dGMP (*26*)	phosphorus is 8.8 ± 1.7 Å from bound Mg^{2+}, and phosphate-O^- is 3.3 ± 0.7 Å from Lys-39-NζH_3^+ (*6*)	
case 2	case 1	case 1	residual dipolar coupling for 53 backbone N−H vectors[a]
case 3	case 1	case 1 + purine C8 = O and N7H hydrogen bonded to Asn-119-NδH_2 and Oδ, respectively, and purine C6 = O hydrogen bonded to Arg-78-NηH_2	
case 4	case 1	case 1 + purine C6 = O and N1H hydrogen bonded to Asn-119-NδH_2 and Oδ, respectively, and purine C8 = O hydrogen bonded to Arg-78-NηH_2	

[a] Residual dipolar coupling values used were those of residues 3−13 of β-strand A; 14−16 of turn 1; 17−18 of β-strand B; 47−56 of α-helix I; 65−68 of loop 2; 69−72, 74 of β-strand C; 79−88 of β-strand D; and 119−120, 122−129 of α-helix II. Omitted were prolines, residues with unresolved signals, and residues in long loops.

Structural Calculations. Distance restraints of 1.8−2.8, 1.8−3.2, and 1.8−5.0 Å were employed for NOE cross-peaks of strong, medium, and weak intensity, respectively, as observed in the NOESY spectra. Additional distance increments of 0.5, 1.0, and 2.3 Å were added to those restraints obtained from NOEs involving degenerate geminal protons, methyl groups, and ring δ- and ϵ-protons, respectively. In addition, 186 ϕ and ψ angle restraints for 93 residues were derived from the ^{15}N, Hα, Cα, and Cβ chemical shifts using the program TALOS (*24*). The enzyme-bound metal (Mg^{2+}) was coordinated to side-chain carboxylate groups of Glu-53, 56, and 57 and the backbone carbonyl group of Gly-38, as determined previously (*6*, *7*).

Torsion-angle simulated annealing (*25*) and refinement calculations were performed with the program CNS 1.1 (*26*) operating on a Silicon Graphics R10000 computer and a Pentium-Linux workstation. All atoms of the 129 amino acid protein, one Mg^{2+} ion, and the 8-oxo-dGMP product were included in the structure calculations. Fifty structures were calculated from an initial extended conformation using a protocol similar to that recommended by Brunger and coworkers (*25*). The initial heating, at 50 000 K, was performed in 1000 steps over a time of 15 ps, using torsion-angle dynamics. The weighting factors for the NOEs, dihedral angles, and van der Waals energies were set to 150, 100, and 0.1, respectively. The first cooling stage, from 50 000 to 0 K, was carried out for 600 ps in 40 000 steps, using torsion-angle dynamics, and linearly increasing the van der Waals weighting factor from 0.1 to 0.5. The second cooling stage, from 2000 to 0 K for 50 ps, involved 10 000 steps and used Cartesian dynamics in which the weighting factors for the NOEs and dihedral angles were increased to 75 and 400, respectively, and the van der Waals weighting factor increased linearly from 1 to 4. The best structure as judged by overall violations and total energy was selected and used to calculate 50 new structures, as outlined above, but with temperatures of 2500 K for the initial heating (1000 steps, 15 ps), from 2500 to 0 K for the first cooling (10 000 steps, 150 ps), and 1000 to 0 K for the second cooling (5000 steps, 25 ps).

The best 33 of 50 structures were selected on the basis of NOE violations ≤0.35 Å, dihedral and bond angle violations ≤10°, and total energy ≤600 kcal/mol. These 33 structures were further refined individually, using temperatures of 1800 K (1000 steps, 15 ps), 1800 to 0 K (6000 steps, 90 ps), and 1000 to 0 K (5000 steps, 25 ps) for the initial heating and the first and second cooling steps, respectively. From this refinement, the best 20 structures were selected on the basis of NOE violations ≤0.25 Å, dihedral and bond angle violations ≤5°, and total energies ≤450 kcal/mol. Because of the lack of a carbon-bound proton on C-8 of the purine ring of 8-oxo-dGMP, intramolecular NOE distance restraints used to define the conformation of MutT-bound 8-oxo-dGMP were unobtainable. Hence, those previously measured for MutT-bound dGMP, together with the resulting dihedral angles for bound dGMP, were used (*27*). The conformation of bound dGMP was very similar to that obtained for bound AMPCPP (*27*). Restraints were added that weakly oriented 8-oxo-dGMP by setting the distances from its phosphorus to the enzyme-bound divalent cation and to Lys-39-Nζ in agreement with those found for bound AMPCPP (*6*). These additional restraints are listed in Table 1 as case 1 and are justified in Results and Discussion.

A second set of structures was obtained with the restraints of case 1, together with restraints provided by the residual dipolar coupling values of 53 backbone N−H vectors (case 2, Table 1) (*28*, *29*) by refining the previous 33 structures, with the weighting factor for the dipolar coupling restraints varying linearly from 0.001 to 1.0. The axial (D_a) and rhombic (R) components of the alignment tensor were estimated from a distribution or histogram of the dipolar coupling constants, as described (*30*). The best values of D_a (−13 ± 1 Hz) and R (0.43 ± 0.05) were found by varying these parameters within their uncertainties, monitoring the total energies and mean pairwise RMSD values of the computed, refined, protein structures (*31*). The parameters D_a and R required for such refinements are uniquely determined by this method (*30*, *31*). One family of structures was obtained, from which the lowest energy structure was further refined by repeating this protocol, but with starting temperatures of 1000 K. The 20 best structures with the lowest energies and no NOE, dihedral, or bond angle violations above the thresholds mentioned above were selected, resulting in lower RMSD values (case 2, Table 1).

Further restraints to orient 8-oxo-dGMP were added to case 1, on the basis of NMR and mutational studies[2] that

Table 2: Restraints and Structural Statistics for the MutT-Mg^{2+}-8-oxo-dGMP Complex

Restraints	
intraresidue NOEs	669
sequential NOEs (i to $i+1$)	472
medium NOEs (i to $i+2-4$)	183
long range (i to $i>4$)	422
hydrogen bonds (2 per H-bond)	82
φ and ψ angles (TALOS)	186
total NOEs	1746
NOE restraints/residue	13.5
Results (averaged from 20 structures)	
total energy (kcal/mol)	≤450
vdw energy (kcal/mol)	≤151
NOE (kcal/mol)	≤120
Restraint Violations	
NOEs (≥0.25 Å)	0
dihedral angles (≥5°)	0
angles (≥5°)	0

RMSD of Restraint Violations

	case 1[a]	case 2	case 3	case 4
bonds	$0.0028 \pm 9.0e^{-5}$	$0.0028 \pm 7e^{-5}$	$0.003 \pm 6e^{-5}$	$0.003 \pm 7e^{-5}$
angles	0.49 ± 0.009	0.58 ± 0.009	0.48 ± 0.007	0.47 ± 0.006
NOEs	$0.02 \pm 8.0e^{-4}$	$0.03 \pm 6.0e^{-4}$	$0.08 \pm 6.0e^{-4}$	$0.02 \pm 5.0e^{-4}$
dihedrals	0.77 ± 0.04	1.15 ± 0.05	0.59 ± 0.02	0.60 ± 0.03
impropers	0.43 ± 0.03	0.61 ± 0.06	0.37 ± 0.01	0.36 ± 0.07

Pairwise RMSD of Backbone Cα,C,N Superposition for 20 Structures (Å)

	case 1	case 2	case 3	case 4
secondary elements (2°)[b]	0.65 ± 0.12	0.49 ± 0.11	0.59 ± 0.13	0.60 ± 0.11
2° + 8-oxo-dGMP	1.52 ± 0.46	0.86 ± 0.28	0.63 ± 0.15	0.70 ± 0.13
residues 1−129	0.98 ± 0.15	0.84 ± 0.21	0.86 ± 0.15	0.89 ± 0.16
residues 1−129 + 8-oxo-dGMP	1.42 ± 0.30	1.00 ± 0.21	0.87 ± 0.16	0.91 ± 0.15
8-oxo-dGMP	2.42 ± 0.86	2.48 ± 1.75	0.78 ± 0.64	0.92 ± 0.89

Ramachandran Plot Analysis for 20 Calculated Structures[c]

residues (%)	case 1	case 2	case 3	case 4
most favored regions	70.6	70.6	72.7	71.8
additionally allowed regions	22.5	21.1	20.8	21.9
generously allowed regions	4.0	5.1	5.0	4.1
disallowed regions	3.0	3.2	1.5	2.3

[a] See Table 1 and text for description of cases 1−4. [b] Residues superpositioned: 2−13, 17−22, 48−58, 69−75, 79−89, 102−106, and 120−128. [c] Ramachandran plots were generated with Procheck-NMR (*36*).

permitted hydrogen bonding from C8 = O and N7H of the purine ring of 8-oxo-dGMP to the side-chain N$\delta$$H_2$ and Oδ of Asn-119, respectively. Similarly, hydrogen bond restraints were added between C6 = O of 8-oxo-dGMP and either NϵH or N$\eta$$H_2$ of Arg-78, the only charged residue near the purine ring of the bound nucleotide (case 3, Table 1). Separate computations were made with the opposite orientation of the purine ring (i.e., with C6 = O and N1H of bound 8-oxo-dGMP approaching the N$\delta$$H_2$ and Oδ of Asn-119, respectively, and with C8 = O of the purine ring approaching either the NϵH or N$\eta$$H_2$ of Arg-78 (case 4, Table 1)). These additional restraints had small (case 3) or no effects (case 4) on the protein structure. Case 2, with the lowest mean pairwise RMSD, was considered the best structure (Table 2).

H/D Exchange Studies. Hydrogen/deuterium exchange rates were determined at 23° on four samples: free MutT, MutT-Mg^{2+}, MutT-Mg^{2+}-dGMP, and MutT-Mg^{2+}-8-oxo-dGMP. Each sample contained 1.0 mM MutT, 4 mM d_{11}-Tris-HCl, (pH 7.5 in H_2O), 21 mM NaCl, and 0.34 mM NaN_3 in 10% D_2O. In addition to the above, to maintain an essentially constant concentration of free Mg^{2+}, the MutT-Mg^{2+} sample contained 15 mM $MgCl_2$, the MutT-Mg^{2+}-dGMP sample contained 35 mM $MgCl_2$ and 20 mM dGMP, and the MutT-Mg^{2+}-8-oxo-dGMP sample contained 15 mM $MgCl_2$ and 1.3 mM 8-oxo-dGMP.

HSQC spectra of MutT in 90% H_2O/10% D_2O were first collected for 5 min (4 scans, 64 t_1 increments, and 0.8 s relaxation delay) and for 20 min (16 scans, 64 t_1 increments, 1.0 s relaxation delay). The protein samples were then lyophilized and dissolved in 99.9% D_2O to initiate the

[2] In preliminary mutagenesis studies, the highly active N119D and N119A mutants showed large 37- and 1650-fold increases, respectively, in the K_I^{slope} of 8-oxo-dGMP, indicating much weaker binding of this nucleotide to these mutants, while only 2−4-fold increases in K_I^{slope} of dGMP and dAMP were found. These results suggest hydrogen bonding of Asn-119 to 8-oxo-dGMP but much weaker interactions with dGMP or dAMP. Also, the fully active R78A mutant showed a 7-fold increase in the K_I^{slope} of 8-oxo-dGMP but only 3.0- and 1.4-fold increases in K_I^{slope} of dGMP and dAMP, respectively, suggesting weak interaction of Arg-78 with 8-oxo-dGMP, weaker interaction of Arg-78 with dGMP, and no interaction of Arg-78 with dAMP (V. Saraswat and A. S. Mildvan, unpublished observations).

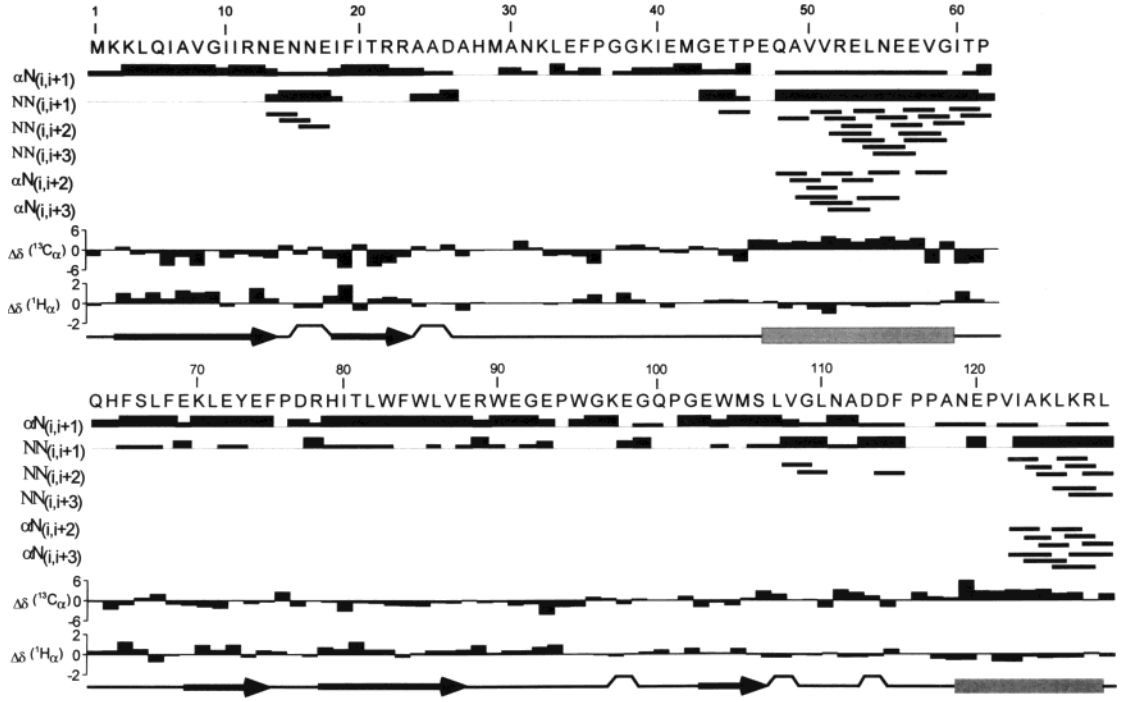

FIGURE 1: Summary of near neighbor backbone interproton NOEs and secondary structural elements of the MutT-Mg^{2+}-8-oxo-dGMP complex. The thicknesses of the lines indicate the intensities of the NOEs as strong, medium, and weak. Chemical shift differences of the Cα and Hα resonances from random coil values are shown to be consistent with the NOE-derived secondary structure. Below is shown the secondary structure with arrows indicating β-strands, shaded rectangles indicating α-helices, inverted cups indicating turns, and lines indicating loops.

exchange, and 5 min HSQC spectra were sequentially collected for 1 h after an initial delay of 12 min for the NMR setup. Next, 20 min HSQC spectra were collected every hour for 24 h and every 3−6 h for the next 100 h. The data were processed with nmrPipe, and peak intensities were analyzed with NMRview. The ratios of the peak intensities collected for 5 and 20 min in 90% H_2O were used to normalize the intensities of peaks for data collected every 5 min in D_2O. Measurements of the decrease in peak intensities with time were fit to a one parameter first-order equation using the Grafit 1.0 program. The NH exchange rates for each amino acid residue were then normalized with respect to the H/D exchange rates of free unstructured amino acids of the same type (*32*) to calculate the protection (slowing) factors, using an Excel spreadsheet provided by Dr. S. W. Englander (University of Pennsylvania).

RESULTS AND DISCUSSION

Resonance Assignments. The large changes in backbone ^{15}N and NH chemical shifts of MutT induced by the binding of 8-oxo-dGMP (*5*) necessitated the reassignment of all resonances (Table S1, Supporting Information). Sequence-specific backbone assignments were made from the 3-D HNCA, HNCACB, and 3-D ^1H-^{15}N-NOESY-HSQC spectra. The HNCA spectrum was instrumental in identifying connectivities between residues that were not part of a β-strand or α-helix. TOCSY cross-peak patterns together with Cα and Cβ chemical shifts from the HNCACB experiment facilitated amino acid identification. Side-chain assignments were made primarily from the ^1H-^{15}N-TOCSY-HSQC spectrum. The TOCSY data were sufficient to make the side-chain proton assignments listed in Table S1 (Supporting Information) when supplemented by the 3-D ^1H-^{13}C NOESY HSQC spectra. The latter permit the distinction between β- and γ-methylene ^{13}C and protons and γ- and δ-methyl ^{13}C and protons of Ile residues. Leu and Val methyl ^{13}C and protons were assigned on the basis of NOE patterns in 3-D ^1H-^{13}C NOESY HSQC spectra. Aromatic protons were assigned from the 2-D NOESY and TOCSY data. Eight of the nine prolines were found to be trans from NOE cross-peak patterns in the ^1H-^{13}C-NOESY-HSQC and ^1H-^{15}N-NOESY-HSQC spectra (*33*). However, the conformation of Pro-116, which precedes Pro-117, could not be assigned because of overlapping ^1H and ^{13}C signals. All nine prolines were found to be trans in free MutT (*15*) and in the quaternary MutT-Mg^{2+}(H_2O)-AMPCPP-Mg^{2+} complex (*6*). For 124 of the 129 residues of MutT (96%), backbone ^{15}N, NH, Cα, and Hα resonances were sequence specifically assigned, and side-chain proton resonances were also sequence specifically assigned, in accord with their expected spin systems (Table S1, Supporting Information).

Secondary Structure. The secondary structure of MutT in the enzyme-Mg^{2+}-8-oxo-dGMP complex consists of five β-strands, on the basis of strong Hα-$NH_{(i,i+1)}$ NOEs between residues 2−13, 17−22, 69−75, 79−89, and 102−106; two α-helices, based on strong NH-$NH_{(i,i+1)}$; and weaker NH-$NH_{(i,i+2,3)}$, Hα-H$\beta_{(i,i+3)}$, and Hα-$NH_{(i,i+2-4)}$ NOEs between residues 48−58 and 120−128 (Figure 1). In addition, four long loops were found between residues 26−46, 59−68, 90−102, and 110−120. Analysis of Cα and Hα chemical shifts were also consistent with the NOE derived secondary structures (Figure 1).

Comparison of the secondary structural elements of the MutT-Mg^{2+}-8-oxo-dGMP complex (Figure 1) with those of free MutT (*34*) and the MutT-Mg^{2+}(H_2O)-AMPCPP-Mg^{2+} complex (*6*) show that the same residues are involved in

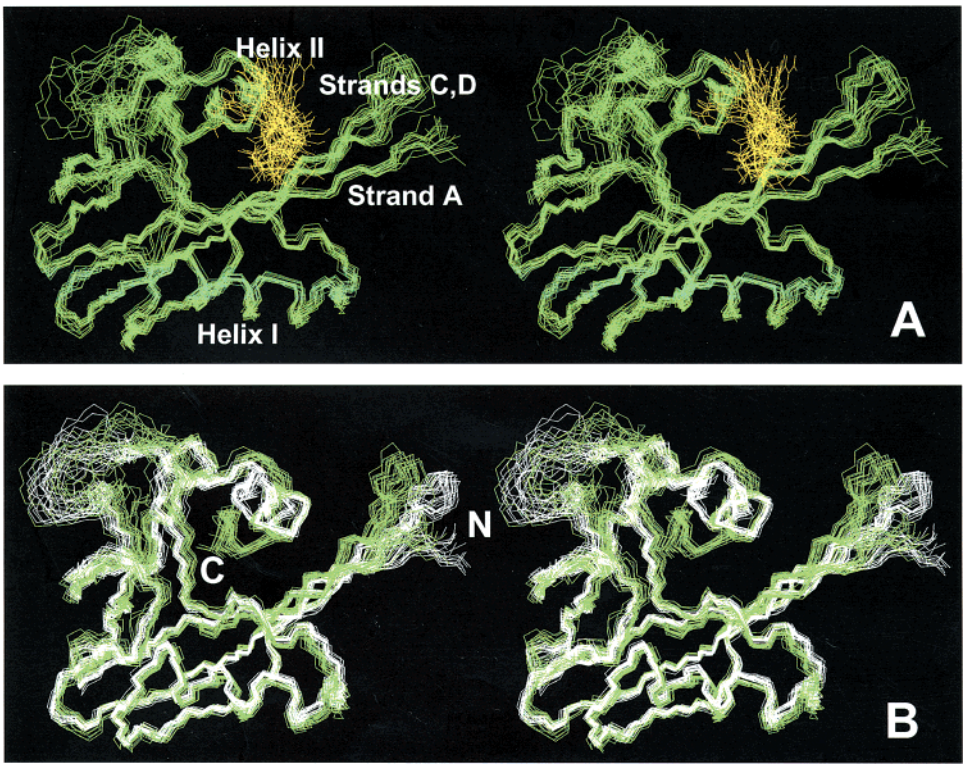

FIGURE 2: Stereopairs of the solution structures of the MutT-Mg^{2+}-8-oxo-dGMP complex. (A) Superposition of backbone Cα, C, and N atoms of 20 computed, converged structures of the MutT-Mg^{2+}-8-oxo-dGMP complex. The carbons of the deoxyribose ring of 8-oxo-dGMP (yellow) are superimposed, but the orientation of the bound nucleotide is only minimally restrained (case 1, Table 1). (B) Superposition of the structure in A (green) onto a set of 20 structures (white) further refined by using residual dipolar coupling of 53 backbone N-H vectors (case 2, Table 1). The nucleotides are omitted for clarity. In all cases, the conformation of bound 8-oxo-dGMP was assumed to be the same as that found for bound dGMP (*27*).

defining the beginnings and ends of the five β-strands and two α-helices. This observation indicates that the binding of the substrate analogue, Mg^{2+}-AMPCPP ($K_D = 284\ \mu M$) (*4*), or the product 8-oxo-dGMP ($K_D = 52$ nM) (*5*) did not change the secondary structure of MutT. This result was unexpected with 8-oxo-dGMP, which binds to MutT-Mg^{2+} with a $10^{4.6}$-fold greater affinity than dGMP and a $10^{3.7}$-fold greater affinity than Mg^{2+}AMPCPP (*4*, *5*). The HSQC titrations of MutT-Mg^{2+} with 8-oxo-dGMP confirmed tight binding by showing slow exchange and large chemical shift changes of 62 backbone amide ^{15}N and/or NH resonances widely distributed throughout the protein (*5*).

Divalent Cation Binding Site. The quaternary MutT-Mg^{2+}-(H_2O)-NTP-Mg^{2+} complex requires two divalent cations for catalytic activity, one coordinated by the β- and γ-phosphoryl groups of the NTP substrate and the other coordinated by the enzyme (*4*). In the quaternary MutT-Mg^{2+}-(H_2O)-AMPCPP-Mg^{2+} complex, the enzyme-bound divalent cation was previously found to be coordinated to the carboxylate groups of Glu-56, 57, and 98, the carbonyl group of Gly-38, and to two water molecules, on the basis of paramagnetic effects of Co^{2+} and Mn^{2+} on resonances of side-chain $^{13}COO^-$ groups (*6*), backbone $^{13}C{=}O$ groups (*6*), and water protons (*4*) as well as the effects of mutations (*7*, *35*). In the binary MutT-Mg^{2+} and ternary MutT-Mg^{2+}-(H_2O)-dNMP complexes, the nucleotide-bound divalent cation was not present, and Glu-53 replaced Glu-98 in the coordination sphere of the enzyme-bound metal (*5*, *7*). These latter restraints were employed in the present structure calculations since the ^1H-^{15}N HSQC spectrum of the MutT-Mg^{2+} complex was identical to that previously determined (*35*).

Tertiary Structure Determination. Figure S1, Supporting Information, shows the residue-specific distribution of NOEs. The tertiary structure of MutT in the enzyme-Mg^{2+}-8-oxo-dGMP complex (Figure 2A) was determined from 1746 NOEs (13.5 NOEs/residue) including 422 long-range NOEs and 82 hydrogen-bond restraints (Table 2). In addition, 186 ϕ and ψ values (for 93 residues) were used, derived from backbone ^{15}N, Cα, Hα, and Cβ chemical shifts with the program TALOS (*24*) (Table 2). Figure 2A shows the structure obtained without residual dipolar coupling restraints (case 1, Table 1), and Figure 2B shows the structure obtained with 53 backbone ^{15}N-H residual dipolar coupling restraints (case 2, Table 1), which is discussed in the next section. As indicated by sequential and long-range NOEs and by slowly exchanging hydrogen-bonded protons, the five β-strands of MutT formed a mixed β-sheet with strands A and D parallel, strands A, B, and E antiparallel, and strands C and D antiparallel (Figure S2, Supporting Information). This β-sheet topology is identical to that found in free MutT (*15*, *33*) and in the MutT-Mg^{2+}-(H_2O)-AMPCPP-Mg^{2+} complex (*6*).

Structure calculations with the program CNS (*25*, *26*) yielded 20 converged structures in which NOE violations are ≤0.25 Å, angle violation are ≤5°, and the total energy for each structure is ≤450 kcal/mol (Table 2, Figure 2A). Ramachandran plot analysis of these 20 structures using the program PROCHECK (*36*) showed 92% of the residues in the most favored and allowed regions, 4−5% in the generously allowed region, and 2−3% in disallowed regions (Table 2). The residues in the disallowed regions appear disordered in the protein structure because of fewer NOE restraints (Figure S1, Supporting Information). Superposition

of the backbone Cα, C′, and N atoms for the secondary structured regions yielded a pairwise root-mean-square deviation (RMSD) value of 0.65 ± 0.12 Å (Table 2), indicating a well-defined tertiary structure (Figure 2A). The pairwise RMSD value for the Cα, C′, and N atoms of all residues was 0.98 ± 0.15 Å. The higher RMSD values for the backbone atoms when all residues are included result from a number of short regions (residues 26−30 and 35−37 in loop I, 98−102 in loop III, and 115−118 in loop IV), which are less well-defined because of fewer NOE restraints (Figure 2A).

In the tertiary structure, helix I packs under the lower surface of the β-sheet near the edge of strand A, while helix II packs onto the upper surface of the β-sheet and protrudes away from the protein core (Figure 2A), similar to that found in free MutT (*15*) and in the quaternary MutT-Mg^{2+}-(H_2O)-AMPCPP-Mg^{2+} complex (*6*).

Structural Refinement by Residual Dipolar Coupling. The structure of the protein in the MutT-Mg^{2+}-8-oxo-dGMP complex, with weak intermolecular hydrogen-bonding restraints to the purine ring (Figure 2A) (case 1, Table 1), was further refined by incorporating the residual dipolar couplings of 53 backbone N−H vectors (Figure 2B) (case 2, Table 1). This refinement resulted in a slight lowering of the RMSD from 0.65 to 0.49 Å for the secondary structural components and from 0.98 to 0.84 Å for all residues (Table 2). Hence, case 2 was considered to be the best structure. Interestingly, this refined structure (Figure 2B) revealed small backbone structural changes: a ∼1.5 Å translation of helix II toward the cleft, together with loop 4, which precedes helix II, and small movements of β-strands C and D. These changes will be discussed next.

Comparison of the Tertiary Structures of Free and Complexed MutT. As noted qualitatively above, MutT preserves the relative orientations of its secondary structural elements on interacting with the weak ligand, Mg^{2+}-AMPCPP (K_D = 284 μM (*4*)), or the strong ligand, 8-oxo-dGMP (K_D = 52 nM (*5*)), indicating that the $10^{3.7}$-fold tighter binding of 8-oxo-dGMP does not result from a drastic change in protein structure but rather from more subtle conformational changes (Figure 3). Hence, detailed, quantitative comparisons of the structures of free and complexed MutT were necessary to elucidate such changes. Table 3 shows the numbers of NOEs used for comparing the structures of free MutT, its strong complex with 8-oxo-dGMP, and its weak complex with Mg^{2+}-AMPCPP, as well as the pairwise RMSD values obtained by the superposition of the backbone Cα, C′, and N atoms of pairs of structures. Similar numbers of total NOEs and hydrogen-bond restraints were used for all three structures.

The overall tertiary structure of the MutT-Mg^{2+}-8-oxo-dGMP complex (case 2, Table 1) is qualitatively similar to those of free MutT and to the quaternary MutT-Mg^{2+}-(H_2O)-AMPCPP-Mg^{2+} complex (Figure 3). However, the superposition of backbone Cα, C′, and N atoms of the MutT-Mg^{2+}-8-oxo-dGMP complex onto those of free MutT reveals significant quantitative differences in the positions of the secondary structural elements (Figure 3A,B; Table 3). The pairwise RMSD values for the backbone atoms of the secondary elements and of all residues are 2.91 ± 0.32 and 3.88 ± 0.37 Å, respectively (Table 3), differences that are much greater than the RMSD values of the individual species being compared.

Table 3: Comparison of the Structures of Free MutT, the MutT-Mg^{2+}-(H_2O)-AMPCPP-Mg^{2+} Complex, and the MutT-Mg^{2+}-8-oxo-dGMP Complex

structures	free-MutT	MutT-AMPCPP	MutT-8-oxo-dGMP
total NOEs	1443	1899	1746
intraresidue	390	538	669
sequential range (i to $i+1$)	502	551	472
medium range (i to $i+2-4$)	171	313	183
long range (i to $i>4$)	380	497	422
hydrogen bonds	34	34	41
dihedral angles	65	120	186

Pairwise RMSD of Cα, C, N Atoms for 16 MutT-Mg^{2+}-(H_2O)-AMPCPP-Mg^{2+} Structures (Å)	
secondary elements[a]	0.51 ± 0.07
residues 1−129	0.75 ± 0.11
Pairwise RMSD of Cα, C, N Atoms for 15 Free MutT Structures (Å)	
secondary elements[a]	1.37 ± 0.25
residues 1−129	2.16 ± 0.35
Comparisons of Pairwise RMSD of Backbone Cα, C, N Superpositions (Å)	
20 MutT-Mg^{2+}-8-oxo-dGMP Structures (Case 2) with 16 MutT-Mg^{2+}-(H_2O)-AMPCPP-Mg^{2+} Structures	
secondary elements[a]	2.45 ± 0.16
residues 1−129	3.40 ± 0.18
20 MutT-Mg^{2+}-8-oxo-dGMP Structures (Case 2) with 15 Free MutT Structures	
secondary elements[a]	2.91 ± 0.32
residues 1−129	3.88 ± 0.37
16 MutT-Mg^{2+}-(H_2O)-AMPCPP-Mg^{2+} Structures with 15 Free MutT Structures	
secondary elements[a]	1.64 ± 0.22
residues 1−129	2.55 ± 0.43

[a] Residues superpositioned: 2−13, 17−22, 48−58, 69−75, 79−89, 102−106, and 120−128.

Most notably (Figure 3A,B), helix I in the MutT-Mg^{2+}-8-oxo-dGMP complex is displaced by ∼4.5 Å toward the active site from its position in free MutT. Also, helix II together with loop 4, which precedes helix II, move toward the cleft, resulting in an overall closing of the active site, and the middle of helix II shows a bend. Slight changes in position of the β-strands A, C, and D, which form part of the base of the nucleotide binding cleft, also occur. Loop 3, which contains the reversible metal ligand Glu-98, also shows significant changes in position in the 8-oxo-dGMP complex (Figure 3A,B, lower left).

In contrast, comparison of the MutT-Mg^{2+}-(H_2O)-AMPCPP-Mg^{2+} complex, containing the $10^{3.7}$-fold weaker-binding substrate analogue Mg^{2+}-AMPCPP, with free MutT, shows much smaller structural differences (Figure 3C,D; Table 3). Helix I moved by only ∼2 Å toward the active site cleft upon nucleotide binding; loop 1 moved slightly away from the cleft; and helix II, loops 3 and 4, and β-strands A, C, and D moved little or not at all, in agreement with previous conclusions based on detailed statistical analysis (*6*).

Consistent with these results, a comparison of the protein structure of the MutT-Mg^{2+}-8-oxo-dGMP complex with that of the weaker MutT-Mg^{2+}-(H_2O)-AMPCPP-Mg^{2+} complex

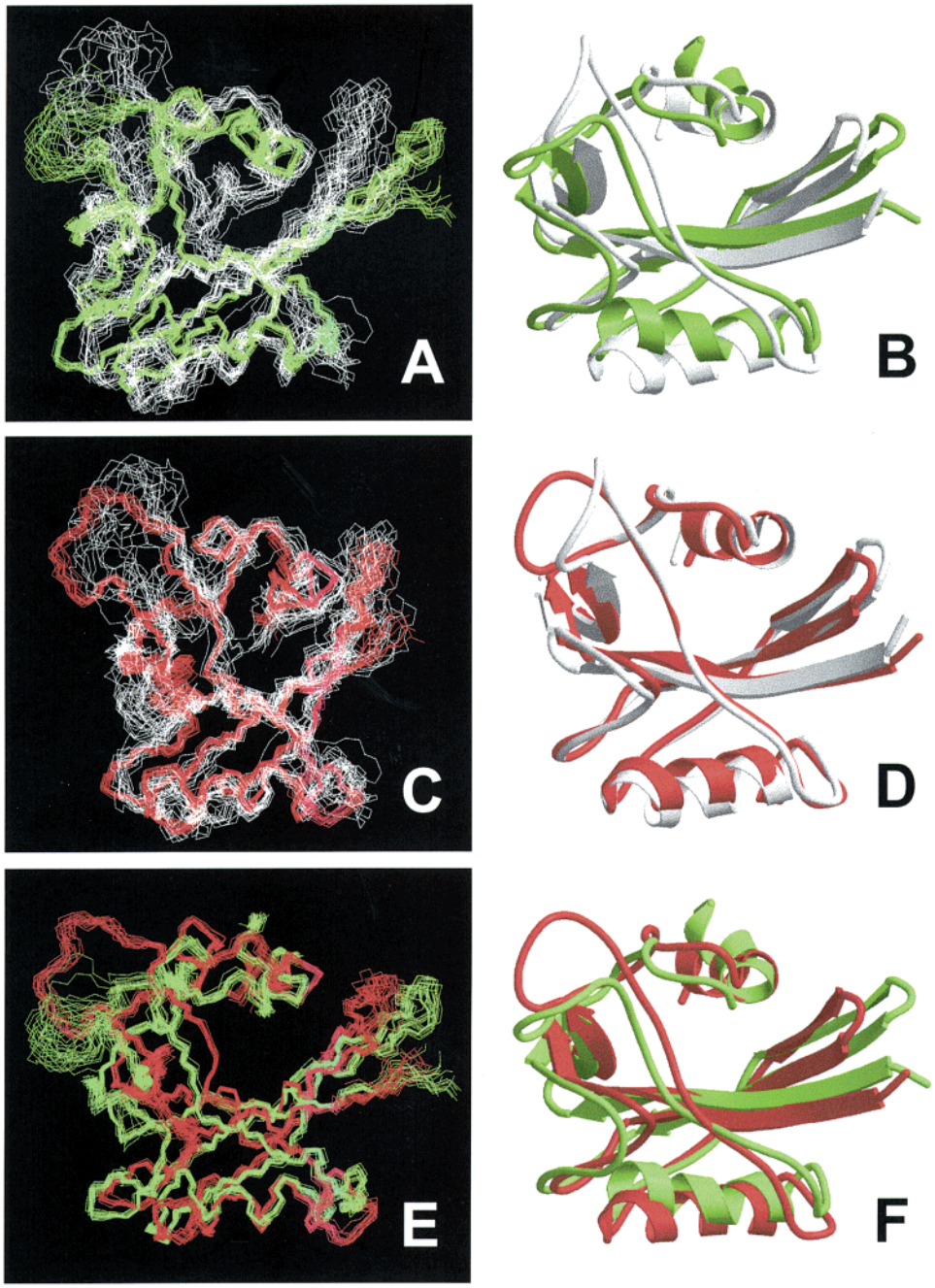

FIGURE 3: Comparisons of the protein structures in free MutT and in its complexes with 8-oxo-dGMP and AMPCPP. Nucleotides are omitted for clarity. (A) Superposition of the backbone Cα, C, and N atoms of an ensemble of 15 computed structures of free MutT (*15*) (white) onto 20 structures of the MutT-Mg^{2+}-8-oxo-dGMP complex (green) (case 2, Table 1). (C) Superposition of free MutT (white, 15 structures) onto the MutT-Mg^{2+}-(H_2O)-AMPCPP-Mg^{2+} complex (*6*) (red, 16 structures). (E) Superposition of the MutT-Mg^{2+}-8-oxo-dGMP complex (green, 20 structures) (case 2, Table 1) onto the MutT-Mg^{2+}-(H_2O)-AMPCPP-Mg^{2+} complex (red, 16 structures). Molscript ribbon superpositions (*42*) of the lowest energy structures from each ensemble are shown in panels B, D, and F with the same color code.

(Figure 3E,F) also shows a narrowing of the nucleotide binding cleft in the 8-oxo-dGMP complex. Helices I and II and loop 4 move toward the active site. The displacement of helix I is smaller (~2.5 Å), while those of helix II, loop 4, and β-strands A, C, and D are similar to those found on comparing the MutT-Mg^{2+}-8-oxo-dGMP complex with the free enzyme. The pairwise RMSD values of the backbone atoms for the secondary structural elements and for all residues are 2.45 ± 0.16 and 3.40 ± 0.18 Å, respectively, which greatly exceed the RMSD values of the individual species being compared (Table 3).

Hence, the binding of 8-oxo-dGMP induces greater conformational changes in MutT than does the binding of Mg^{2+}AMPCPP, most notably in the positions of helices I and II and loop 4, which close in on the nucleotide binding site (Figure 3E,F). These structural differences may well contribute to the $10^{3.7}$-fold greater affinity of MutT for 8-oxo-dGMP. The mechanistically related Nudix enzyme Ap_4A hydrolase (*37*) also shows significant conformational changes on binding the reaction product ATP, in the presence of saturating $MgCl_2$ and NaF (*38*). Although the conformational changes of Ap_4A hydrolase differ in detail from those of

Table 4: Comparison of Intermolecular NOEs from the MutT Enzyme to the Sugar Protons of the Bound Nucleotide in the 8-Oxo-dGMP[a] and AMPCPP[b] Complexes, in the Presence of Saturating $MgCl_2$

	8-oxo-dGMP[a]		AMPCPP[b,c]	
sugar	MutT δ		MutT δ	
proton	($^1H/^{13}C$)	assignment	($^1H/^{13}C$)	assignment[b]
H1′	0.73/12.5	I6Hδ_{Me}	1.70/46.3	L4H$\beta_{1,2}$
	0.88/14.9	I80Hδ_{Me}	1.62/28.5	L4Hγ
			0.94/25.7	L4H$\delta_{Me1,2}$
H2′(2″)	1.68/41.5	I80Hβ	0.67/12.9	I6Hδ_{Me}
	0.96/18.8	I80Hγ_{Me}		
	0.88/14.9	I80Hδ_{Me}		
	0.97/25.6	L82Hδ_{Me1}		
H3′	0.73/12.5	I6Hδ_{Me}	0.93/25.6	L4H$\delta_{Me1,2}$
	0.88/14.9	I80Hδ_{Me}		
H4′			1.68/46.4	L4H$\beta_{1,2}$
			0.94/25.8	L4H$\delta_{Me1,2}$
			1.76/29.8	K39H$\delta_{1,2}$
H5′(5″)	0.49/17.8	I6Hγ_{Me}	1.68/46.2	L4H$\beta_{1,2}$
	0.73/12.5	I6Hδ_{Me}	0.94/25.6	L4H$\delta_{Me1,2}$

[a] All NOEs to 8-oxo-dGMP were weak to medium with signal/noise ratios of 2.8−3.2. [b] From ref *6*. [c] Also detected in the AMPCPP complex were three NOEs to adenine-H8 from L4 and two from I6, as well as four NOEs to adenine-H2 from I80 (*6*).

Table 5: Arginine-$^{15}N\epsilon$ and -NϵH Chemical Shifts (in ppm) from ^1H-^{15}N HSQC Spectra of MutT Complexes at 5°, pH 7.5

	MutT-Mg^{2+}	MutT-Mg^{2+}-8-oxo-dGMP	
resonance	δ ($^1H/^{15}N$)	δ ($^1H/^{15}N$)	$\Delta\delta$ ($^1H/^{15}N$)
A	7.26/83.51	7.32/83.59	0.06/0.08
B	7.16/83.35	6.99/86.61	−0.17/3.26
C	7.18/84.10	7.14/82.95	−0.04/−1.15
D	6.68/89.04	6.64/88.92	−0.04/−0.12
E	8.36/87.93	8.21/86.89	−0.15/−1.04
F		7.24/82.02	
G		7.38/90.32	

MutT, they also narrow the nucleotide binding cleft (*38*). The requirement for NaF and $MgCl_2$ to form the slowly exchanging ATP complex of Ap_4A hydrolase suggests the formation of a trigonal bipyramidal transition state analogue ATP-O-Mg(F^-)$_3$-OH_2 on this enzyme (*39*).

8-Oxo-dGMP Binding Site. The analysis of the $^{13}C/^{12}C$-edited-NOE-filtered and ^1H-^{13}C-NOESY-HSQC spectra yielded a total of 12 weak intermolecular NOEs from six of the seven carbon-bound protons of the deoxyribose ring to six proton groups of the protein, assigned as described in Experimental Procedures, that defined the deoxyribose binding site of 8-oxo-dGMP. Comparison of these NOEs with NOEs from MutT to AMPCPP (*6*) revealed different but overlapping interactions for the two nucleotides (Table 4), consistent with overlapping but nonidentical binding sites. Thus, the deoxyribose of 8-oxo-dGMP shows NOEs from Ile-6 of β-strand A, and from Ile-80, and Leu-82 of β-strand D, while the ribose of AMPCPP shows NOEs only from Leu-4 and Ile-6 of β-strand A. These NOEs indicate that in comparison with AMPCPP, 8-oxo-dGMP is translated by ~2 Å from β-strand A toward the adjacent and parallel β-strand D, approaching the amino terminus of helix II (Figure 2A).

While the NOEs in Table 4 defined the position of bound 8-oxo-dGMP (Figure 2A), additional restraints were required to define its conformation and orientation (Figure 4). Because of the absence of nonexchangeable protons on the purine ring of 8-oxo-dGMP, no intramolecular NOEs between the base and the deoxyribose were observed. Hence, the con-

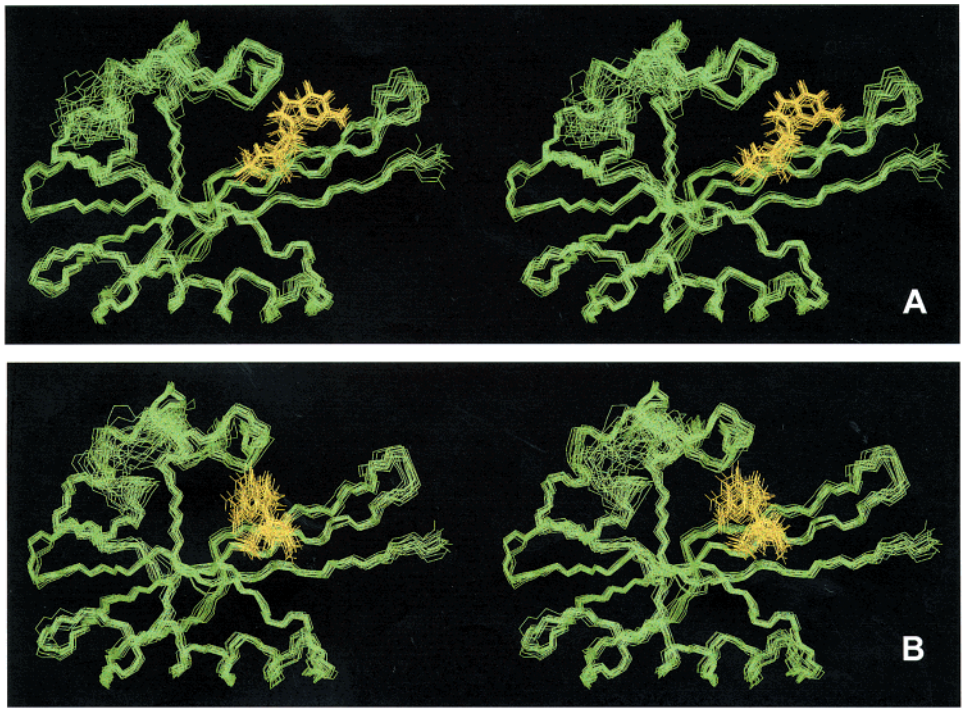

FIGURE 4: Stereopairs showing the conformations and alternate locations of bound 8-oxo-dGMP in the MutT-Mg^{2+}-8-oxo-dGMP complex. (A) Case 3 (Table 1): superposition of 20 structures restrained by assuming hydrogen bonding of the purine C8 = O and N7-H of 8-oxo-dGMP to Asn-119-NδH_2 and Oδ, respectively, and of the purine C6 = O to Arg-78-NηH_2. (B) Case 4 (Table 1): superposition of 20 structures restrained by assuming the opposite hydrogen bonding of the purine C6 = O and N1H to Asn-119-NδH_2 and Oδ, respectively, and the purine C8 = O to Arg-78-NηH_2. In all cases, the conformation of bound 8-oxo-dGMP was assumed to be the same as that found for bound dGMP (*27*).

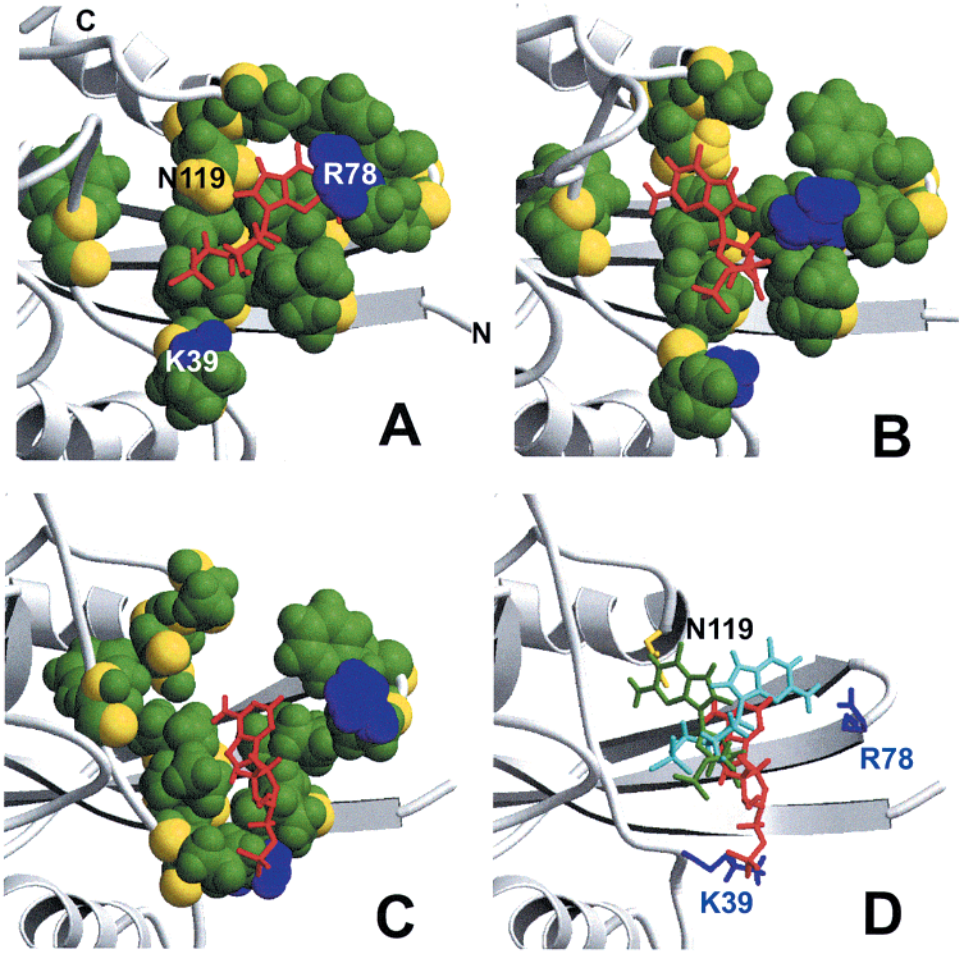

FIGURE 5: Comparison of the overlapping nucleotide binding sites on MutT for 8-oxo-dGMP and for the AMP moiety of AMPCPP in their respective lowest energy structures. (A) 8-Oxo-dGMP, case 3. (B) 8-Oxo-dGMP, case 4. (C) The AMP moiety of AMPCPP (*6*). Space-filling Molscript models (*42*) are shown with hydrophobic groups in green, polar groups in yellow, cationic groups in blue, and anionic groups in red. Note the hydrophobic character of the site. (D) Superposition of the residues in contact with the bound nucleotides in panels A−C showing the relative positions of 8-oxo-dGMP, case 3 (cyan); 8-oxo-dGMP, case 4 (green); and AMP (red). Cases are defined in Table 1 and in the text.

formation of bound 8-oxo-dGMP was assumed to be the same as that found for bound dGMP, with a high anti-glycosidic torsional angle ($\chi = 73 \pm 9°$) and a C1′-endo sugar pucker ($\delta = 118 \pm 11°$) (*27*). These torsional angles were very similar to those found for bound AMPCPP (*27*). To facilitate the orientation of bound 8-oxo-dGMP, its phosphorus was restrained to be 8.0 ± 1.7 Å from the enzyme-bound divalent cation, and one of its phosphate oxygens was restrained to be 3.3 ± 0.7 Å from Nζ of the catalytic residue, Lys-39, distances very similar to those found in the AMPCPP complex (*6*). Collectively, these restraints are referred to as case 1 (Table 1).

Further evidence that 8-oxo-dGMP and NTPs bind in the same substrate binding cleft, in addition to the intermolecular NOEs (Table 4) and the previously detected kinetic competition with dGTP (*5*), is the disappearance of both side-chain -NδH_2 resonances of Asn-119 in the ^{15}N HSQC spectrum of the MutT-Mg^{2+}-8-oxo-dGMP complex. No downfield shifted proton resonances (>11 ppm) appeared at 5 or 25° that would indicate unusually strong hydrogen bonds between Asn-119 and the C8 = O or the N7-H of the purine ring of 8-oxo-dGMP, although these are not excluded. Previously, it was found that the binding of AMPCPP resulted in a small upfield shift (−0.05 ppm) of the downfield of the two NδH_2 resonances of Asn-119, while the binding of dGTP resulted in a larger downfield shift of this resonance (0.54 ppm), suggesting an interaction of the guanine base with Asn-119-NH_2 (*6*). Also, the exchange rate with solvent of the backbone NH of Asn-119 slowed by ~10^6-fold in the 8-oxo-dGMP complex in comparison with all other complexes of MutT.

Preliminary mutagenesis studies[2] suggest hydrogen bonding of Asn-119 to 8-oxo-dGMP but much weaker interactions of this residue with dGMP or dAMP. Accordingly, in separate structure calculations (Figure 4A), the distances from Asn-119-NδH_2 and Oδ to the C8 = O and N7H, respectively, of 8-oxo-dGMP were restrained to 2.8 ± 0.2 Å, with small effects on the backbone structure of the protein.

The NOEs between MutT and the deoxyribose ring of 8-oxo-dGMP (Table 4), initial modeling of the complex, and preliminary mutagenesis studies[2] also suggest that acceptor atoms of the 8-oxo-guanine ring can approach and accept a hydrogen bond from the side-chain guanidinium of Arg-78 (the only Arg in the nucleotide binding cleft). Accordingly, in the structure calculations, the distances from C6 = O of 8-oxo-dGMP to either the NϵH or the NηH_2 of Arg-78 were restrained to 2.8 ± 0.2 Å, with small effects on the backbone structure of the protein (Figure 4A). Collectively, these

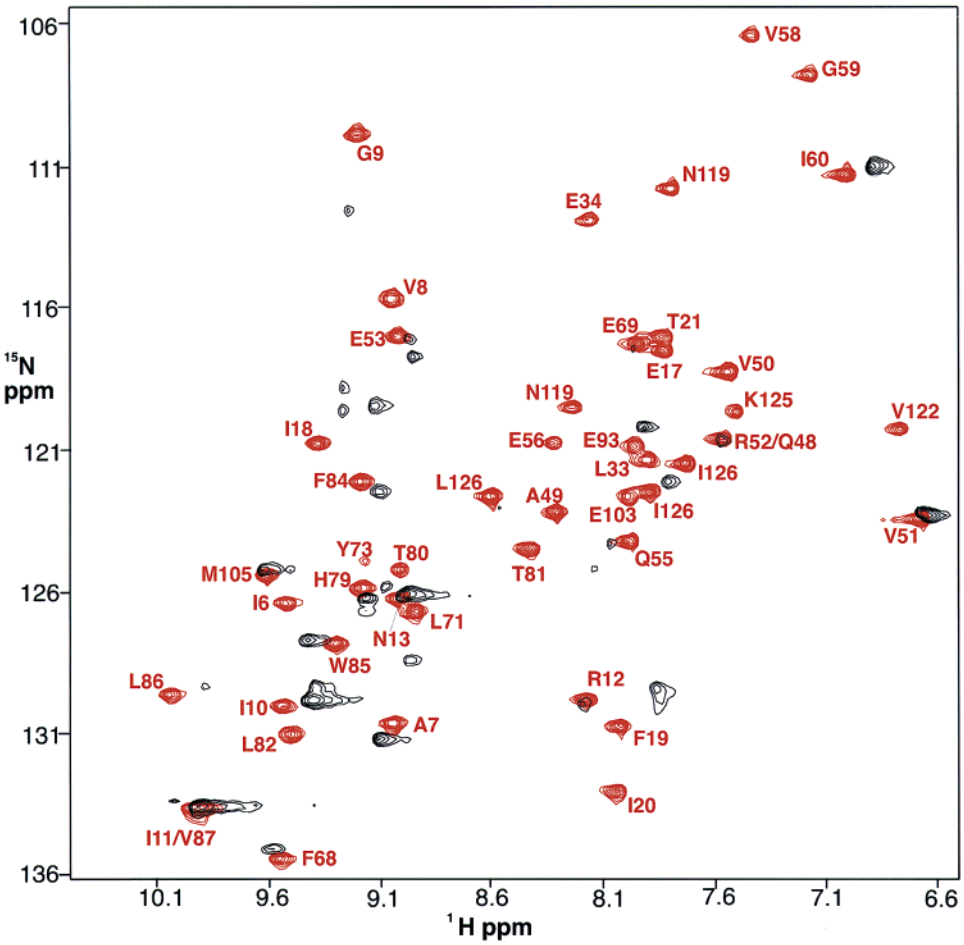

FIGURE 6: ^{1}H-^{15}N HSQC spectra of MutT-Mg^{2+}-8-oxo-dGMP (red) and MutT-Mg^{2+}-dGMP (black) collected after being in 100% D_2O for 62 and 51 h, respectively, at 23°, pH 7.5. Components present were 1.3 mM 8-oxo-dGMP, 1.0 mM MutT, and 15 mM $MgCl_2$; or 20 mM dGMP, 1.0 mM MutT, and 35 mM $MgCl_2$ together with 3.4 mM Tris d_{11}Cl, pH 7.5, 18 mM NaCl, and 0.3 mM NaN_3 in 99.96% D_2O. Assigned resonances of the MutT-Mg^{2+}-8-oxo-dGMP complex are labeled. The nonexchanged spectra are shown in Figure 7 of ref *5*.

additional hydrogen-bonding restraints between 8-oxo-dGMP and the two residues, Asn-119 and Arg-78, are referred to as case 3 (Table 1).

In other calculations, the opposite orientation of the purine ring was assumed, with Asn-119-Nδ and Oδ approaching the C6 = O and N1H, respectively, of 8-oxo-dGMP, and Arg-78-NϵH or NηH$_2$ approaching the C8 = O of 8-oxo-dGMP (Figure 4B), with no significant effects on the backbone structure of the protein. These alternative restraints are referred to as case 4 (Table 1).

MutT contains seven Arg residues of which five Arg-NϵH resonances were detected in a ^{1}H-^{15}N HSQC spectrum of the MutT-Mg^{2+} complex (Table 5). The binding of 8-oxo-dGMP to the MutT-Mg^{2+} complex induced shifts in these signals and the appearance of two additional Arg-NϵH resonances (Table 5). Most of the Arg-NϵH proton shifts induced by the binding of 8-oxo-dGMP were upfield, arguing against increased NϵH hydrogen-bond donation. However, the appearance of two new Arg-NϵH resonances, presumably because of slowed exchange with the solvent, suggests increased NϵH hydrogen-bond donation by these two Arg residues. A hydrogen bond between Arg-78 and 8-oxo-dGMP could contribute to the $10^{4.6}$-fold tighter binding of 8-oxo-dGMP over dGMP. These points are being studied by the effects of Arg mutations on NMR spectra and on nucleotide binding.[2]

Figure 5A,B compares in detail the locations and enzymatic environments of enzyme-bound 8-oxo-dGMP in the two alternative orientations defined by the restraints of cases 3 and 4, respectively (Table 1).[3] For comparison, Figure 5C shows the location and enzymatic environment of the AMP moiety of AMPCPP (*6*). Figure 5D, obtained by superimposing the protein residues in Figures 5A−C, which are in contact with the bound nucleotides, indicates that 8-oxo-dGMP and the AMP moiety of AMPCPP bind to overlapping sites. These sites are predominantly hydrophobic (Figure 5A−C). The residues that line the nucleotide binding cleft are located on the surface of β-strands A, C, and D, loop 1, and the amino terminus of helix II. They consist mainly of the apolar residues Leu-4, Ile-41, Tyr-73, Phe-75, Ile-80, and Leu-82. The only charged or polar residues present within 4.8 Å of bound 8-oxo-dGMP are Lys-3, Lys-39, Arg-78, and Asn-119.

The orientation of MutT-bound 8-oxo-dGMP defined by case 3 (Table 1, Figures 4A and 5A) buries an average of 78 ± 3% of the total surface area of the nucleotide (530 ± 8 Å^2), as measured by the program MSMS (*40*). The

[3] Modeling of a pyrophosphoryl group onto 8-oxo-dGMP in the orientations defined by both case 3 (Figure 5A) and case 4 (Figure 5B) permitted the resulting 8-oxo-dGTP molecules to reach the reaction center and form potentially productive complexes.

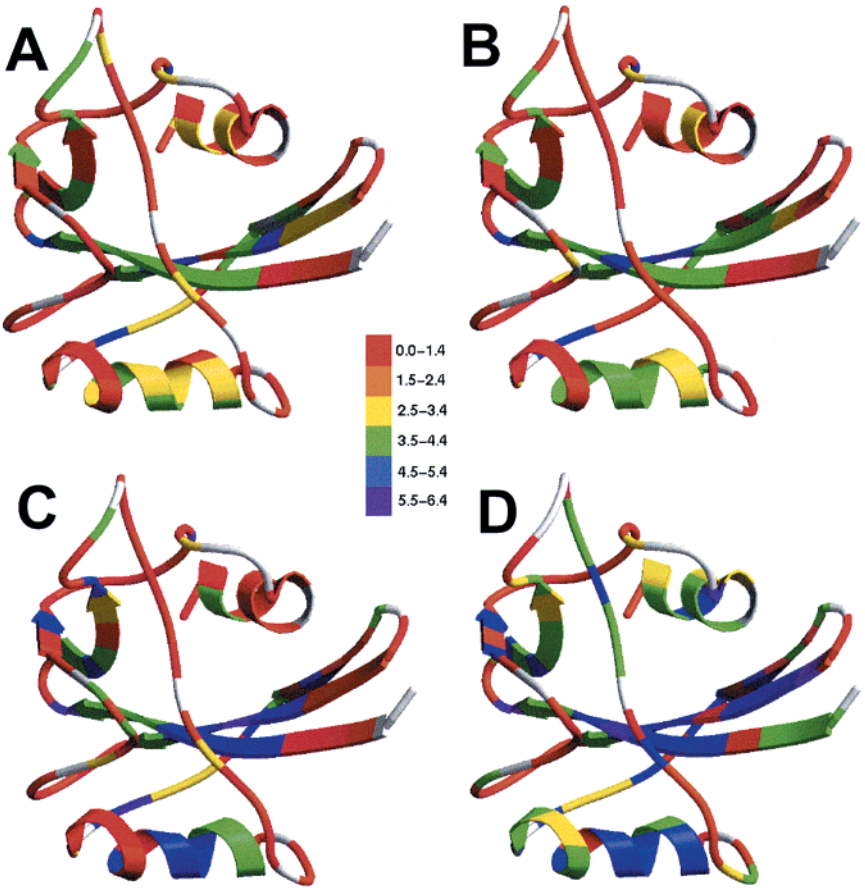

FIGURE 7: Protection (slowing) factors for backbone NH/ND exchange of individual residues of free MutT and its complexes at pH 7.5 and 23°. Molscript ribbon drawings of MutT (*42*) color-coded to indicate the log[protection factors] that range from red for little or no protection ($10^{0-1.4}$) to purple for residues that were protected from exchange after 7 days in D_2O ($10^{5.5-6.4}$). White represents residues for which the NH protons were not assigned. Log[protection factors] are shown for (A) free MutT; (B) the MutT-Mg^{2+} complex; (C) the MutT-Mg^{2+}-dGMP complex; and (D) the MutT-Mg^{2+}-8-oxo-dGMP complex.

alternative orientation of bound 8-oxo-dGMP defined by case 4 (Table 1, Figures 4B and 5B) shows slightly less burial, 71 ± 4% of the total nucleotide surface area (546 ± 6 Å^2). In contrast, the AMP moiety of AMPCPP shows only 57 ± 6% burial of its surface area (536 ± 4 Å^2), consistent with the $10^{3.7}$-fold weaker binding of AMPCPP to the enzyme (*4*, *5*).

As noted above, structural refinement of the MutT-Mg^{2+}-8-oxo-dGMP complex by incorporating residual dipolar couplings of 53 backbone N−H vectors (case 2, Table 1) resulted in small structural changes: a ~1.5 Å translation of helix II and loop 4 toward the cleft and small movements of β-strands C and D (Figure 2B). Case 2 was deemed the best structure on the basis of the lowest mean pairwise RMSD values (Table 2). Interestingly, these structural changes were very similar to those found in Figures 4A and 5A (case 3, Table 1), which were generated without residual dipolar coupling by assuming hydrogen bonding from the C8 = O and N7H of the purine ring to Asn-119-NδH$_2$ and Oδ, respectively, and from the C6 = O to Arg-78-NηH$_2$. No such structural changes in the protein backbone were found for case 4 (Figures 4B and 5B) in which the opposite hydrogen bonding pattern was assumed (Table 1). The agreement in backbone structures of the protein derived independently from residual dipolar coupling without specific orientation of the purine ring (Figure 2B), and from a specific orientation of the purine ring without residual dipolar coupling (Figures 4A and 5A), supports the position of 8-oxo-dGMP shown in Figures 4A and 5A (case 3) over that shown in Figures 4B and 5B (case 4).

Hydrogen/Deuterium Exchange Studies. To independently test the hypothesis that the high affinity of MutT for 8-oxo-dGMP might result in part from a closing down or tightening of the enzyme structure, including that of the active site, hydrogen−deuterium (H/D) exchange studies were performed on free MutT and on three of its complexes: MutT-Mg^{2+}, MutT-Mg^{2+}-(H_2O)-dGMP, and MutT-Mg^{2+}-(H_2O)-8-oxo-dGMP at 23° and pH 7.5. A comparison of the ^{1}H-^{15}N HSQC spectra of the MutT-Mg^{2+}-(H_2O)-dGMP and MutT-Mg^{2+}-(H_2O)-8-oxo-dGMP complexes after 51 and 62 h in D_2O, respectively, (Figure 6) shows the 8-oxo-dGMP complex to protect 45 out of 112 resonances from rapid exchange, whereas the dGMP complex protects only 20 resonances out of 115. With free MutT, after 50 h in D_2O, only 11 out of 114 resonances remained, and with the MutT-Mg^{2+} complex 22 out of 115 resonances remained (data not shown).

Exchange Rate Protection Factors for Free MutT and Mg^{2+}-MutT. Pseudo-first-order rate constants for the NH exchange of the assigned resonances at 23° were calculated and compared with exchange rate constants of the same residues when exposed to solvent in small peptides, to yield protection (or slowing) factors (*32*). For free MutT, the protection factors vary from 1, indicating no protection

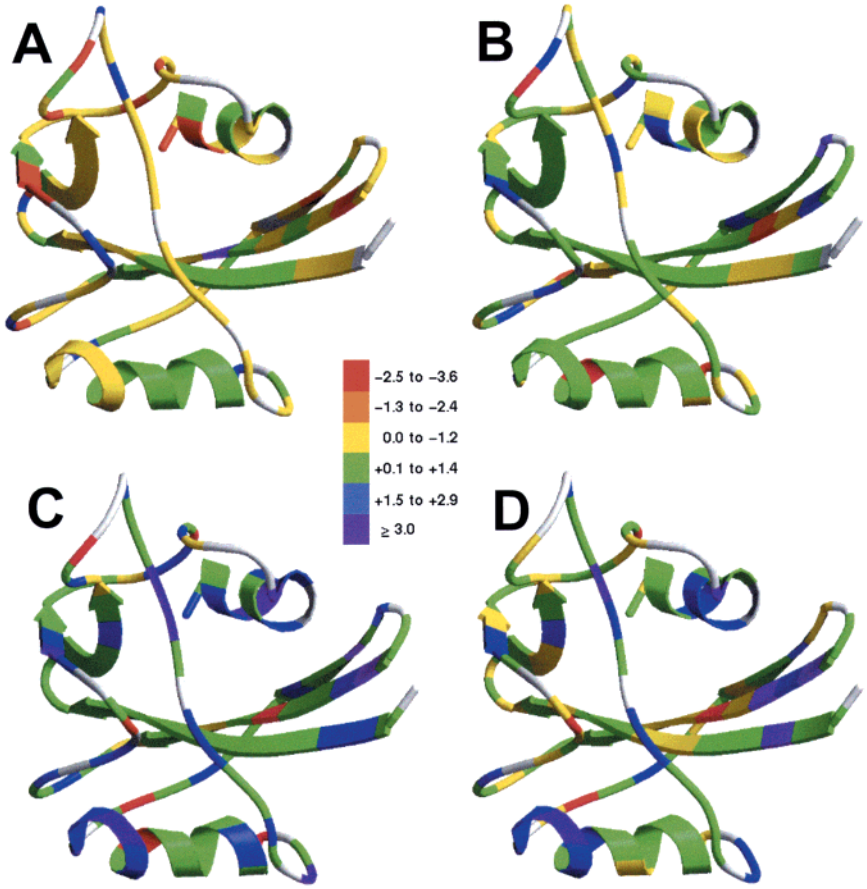

FIGURE 8: Pairwise comparisons of log[protection factors] for residues of free MutT and its complexes. (A) MutT-Mg^{2+} minus free MutT, (B) MutT-Mg^{2+}-dGMP minus MutT-Mg^{2+}, (C) MutT-Mg^{2+}-8-oxo-dGMP minus MutT-Mg^{2+}, and (D) MutT-Mg^{2+}-8-oxo-dGMP minus MutT-Mg^{2+}-dGMP. Note that differences in log[protection factors] are equal to the log[ratio] of protection factors. As indicated by the color code, the difference in log[protection factor] for a residue in two complexes is shown as yellow if the protection factors are nearly equal in the two complexes (Δ[log(PF)] = 0 to −1.2). Those residues that are less protected than in their partner are shown in orange to red, and those that are more protected are shown in green, blue, and purple (Δ[log(PF)] ≥ 3).

against exchange, to 10^6, indicating significant protection, with a majority of amide protons showing values in the $10^{1.5}-10^{4.4}$ range as a result of the protein being folded (Figure 7A). Interestingly, many of the residues from the long loops show protection against exchange, suggesting that their amide protons are not completely exposed.

The addition of Mg^{2+} to MutT increases the protection factors of 26 residues by ~10-fold, notably those in the middle of helix I (Figure 7B). This is reasonable since helix I contains residues that coordinate the metal (Glu-53, 56, and 57). Increased protection factors were also observed for residues on β-strand A and helix II. These effects are seen more clearly in the difference in log[protection factors] (Figure 8A), which is equal to the log[ratio] of the protection factors of MutT-Mg^{2+} and MutT. In Figure 8A, protection factors that showed little change between the two systems ($10^{0.0}-10^{-1.2}$) are colored yellow. Decreases in protection factors (reflecting increases in exchange rates of MutT-Mg^{2+} vs free MutT) are shown in orange and red, and increases in protection factors (reflecting decreases in exchange rates of MutT-Mg^{2+} vs free MutT) are shown in green, blue, and purple.

Exchange Rate Protection Factors for MutT-Mg^{2+}-Nucleotide Complexes. Formation of the MutT-Mg^{2+}-dGMP and MutT-Mg^{2+}-8-oxo-dGMP complexes leads to further slowing of NH exchange for many additional residues (Figure 7C,D). Thus, the binding of dGMP increases the protection factors of residues around the binding cleft, as seen by the strip of blue across strands A and D of the β-sheet and along helix I (Figure 7C). The ratios of protection factors of the MutT-Mg^{2+}-dGMP and MutT-Mg^{2+} complexes (Figure 8B) show that dGMP binding induces ~10-fold slowing of exchange of 20 residues predominantly along helix I and in the nucleotide binding cleft.

In contrast, 8-oxo-dGMP binding protects many residues throughout the entire protein, including those surrounding the nucleotide binding cleft, and by greater factors (Figure 7D). Notably, the backbone NH of Asn-119 exchanges ~10^6-fold slower in the MutT-Mg^{2+}-8-oxo-dGMP complex than in any other complex of MutT, which is part of an overall slowing of exchange that occurs throughout helix II (Figure 7D). Comparison of the protection factors of MutT-Mg^{2+}-8-oxo-dGMP with those of MutT-Mg^{2+} (Figure 8C) shows greater protection by 8-oxo-dGMP for 45 residues by 1−3 orders of magnitude, with 36 residues showing ≥10^2-fold greater protection. Similarly, comparison of the protection factors of the 8-oxo-dGMP and dGMP complexes (Figure 8D) indicates a relative slowing of exchange of 36 residues of the former, by 1−3 orders of magnitude. These diffuse slowing effects (Figures 7 and 8) suggest a general tightening of the protein structure in the 8-oxo-dGMP complex, consistent with the differences seen in the comparisons of

the tertiary structures (Figure 3 and Table 3). The exchange data also suggest a shortening of ~45 backbone hydrogen bonds in the 8-oxo-dGMP complex, which could contribute to the strongly favorable enthalpic contribution ($\Delta H = -32$ kcal/mol) to the free energy of binding of 8-oxo-dGMP ($\Delta G° = -9.8$ kcal/mol) (*5*). The resulting increase in structural order could explain the unfavorable entropy change on binding ($-T\Delta S° = +22$ kcal/mol).

However, since hydrogen-bond lengths do not strictly correlate with protection factors, an alternative explanation of the H/D exchange data must be considered (*41*). As ligands such as 8-oxo-dGMP bind to MutT, the complex assumes a lower energy state in which the local and/or global unfolding rates decrease, diminishing the transient exposure of backbone NH protons to the solvent, thereby slowing exchange. Complexation with Mg^{2+} and nucleotides, especially 8-oxo-dGMP, favors a more tightly folded state of the protein. This lowered energy and more ordered state of the MutT-Mg^{2+}-8-oxo-dGMP complex may also contribute significantly to the tighter binding and the unfavorable $-T\Delta S°$ value observed.

CONCLUSION

The product of the MutT reaction, 8-oxo-dGMP, binds to the MutT-Mg^{2+} complex with a K_D (52 nM) that is $10^{4.6}$-fold lower than that of dGMP, driven by a highly favorable enthalpy change ($\Delta H_{binding} = -32$ kcal/mol), which overcomes an unfavorable entropy change ($-T\Delta S°_{binding} = +22$ kcal/mol) (*5*). The 6 kcal/mol tighter binding of 8-oxo-dGMP than of dGMP appears to correlate with widespread changes in the protein structure as suggested by changes in the backbone ^{15}N and NH chemical shifts of 62 residues distributed throughout the protein (*5*). To directly test this possibility, the solution structure of the MutT-Mg^{2+}-8-oxo-dGMP complex was determined and compared with those of free MutT (*15*) and with the quaternary MutT-Mg^{2+}-(H_2O)-AMPCPP-Mg^{2+} complex (*6*).

While the secondary structures showed no differences, the tertiary structures showed a narrowing of the hydrophobic nucleotide-binding cleft in the 8-oxo-dGMP complex resulting from 2.5−4.5 Å movements of helix I and smaller movements of helix II and loop 4 toward the cleft. Structural refinement of the 8-oxo-dGMP complex with residual dipolar couplings of 53 backbone N−H bond vectors produced additional small structural changes in the positions of helix II, loop 4, and the β-sheet, leading to the best structure as judged by the lowest mean pairwise RMSD values (Table 2). These structural changes were similar to those found without dipolar coupling by assuming a specific orientation of bound 8-oxo-dGMP in which the purine C8 = O and N7H were hydrogen bonded to Asn-119-NδH and Oδ, respectively, and the purine C6 = O was hydrogen bonded to Arg-78-NηH_2. The interactions with Asn-119 and Arg-78 are consistent with preliminary studies of these residues by mutagenesis.[2] The greater burial by MutT of 71−78% of the surface area of 8-oxo-dGMP than that of the AMP moiety of AMPCPP (57%) correlates with the $10^{3.7}$-fold tighter binding of 8-oxo-dGMP.

Formation of the MutT-Mg^{2+}-8-oxo-dGMP complex slowed the backbone NH exchange rates of 45 residues by factors of 10^1−10^3 as compared with those of the same residues in the MutT-Mg^{2+} and the MutT-Mg^{2+}-dGMP complexes, consistent with widespread tightening of the protein structure, including the nucleotide-binding cleft. The slowed H/D exchange rates in the MutT-Mg^{2+}-8-oxo-dGMP complex also suggest a more stable structure. The $10^{4.6}$-fold weaker binding of dGMP to MutT-Mg^{2+} slows the backbone exchange rates of only 20 residues, and by smaller factors of ~10.

Hence, the high affinity of MutT for 8-oxo-dGMP likely results in part from ligand-induced conformation changes that narrow the nucleotide binding site and strengthen numerous backbone hydrogen bonds. Specific hydrogen bonding of the purine C8 = O and N7H of 8-oxo-dGMP by Asn-119 and of the C6 = O by Arg-78 may also contribute significantly to the highly favorable enthalpy of binding. The resulting increased structural order of the MutT-Mg^{2+}-8-oxo-dGMP complex can explain the unfavorable entropy of binding.

ACKNOWLEDGMENT

We thank Drs. Lewis Kay and Ranjith Muhandiram (University of Toronto) for providing pulse sequences and data processing macros used for dipolar coupling measurements, Dr. David Shortle for advice on orienting media, and Dr. C. Cao for helpful discussions of the program CNS. We also thank Dr. S. Walter Englander (University of Pennsylvania) for providing an Excel spreadsheet for calculation of protection factors.

SUPPORTING INFORMATION AVAILABLE

One table (Table S1), showing assignments of the ^1H, ^{13}C, and ^{15}N resonances of MutT in the MutT-Mg^{2+}-8-oxo-dGMP complex, and two figures, Figure S1 showing the number of NOEs involving each residue and Figure S2 showing the β-sheet topology of MutT in the MutT-Mg^{2+}-8-oxo-dGMP complex. This material is available free of charge via the Internet at http://pubs.acs.org.

REFERENCES

1. Bessman, M. J., Frick, D. N., and O'Handley, S. F. (1996) *J. Biol. Chem. 271*, 25059−25062.
2. Weber, D. J., Bhatnagar, S. K., Bullions, L. C., Bessman, M. J., and Mildvan, A. S. (1992) *J. Biol. Chem. 267*, 16939−16942.
3. Mildvan, A. S., Weber, D. J., and Abeygunawardana, C. (1999) *Adv. Enzymol. Relat. Areas Mol. Biol. 73*, 183−207.
4. Frick, D. N., Weber, D. J., Gillespie, J. R., Bessman, M. J., and Mildvan, A. S. (1994) *J. Biol. Chem. 269*, 1794−1803.
5. Saraswat, V., Massiah, M. A., Lopez, G., Amzel, L. M., and Mildvan, A. S. (2002) *Biochemistry 41*, 15566−15577.
6. Lin, J., Abeygunawardana, C., Frick, D. N., Bessman, M. J., and Mildvan, A. S. (1997) *Biochemistry 36*, 1199−1211.
7. Harris, T. K., Wu, G., Massiah, M. A., and Mildvan, A. S. (2000) *Biochemistry 39*, 1655−1674.
8. Maki, H., and Sekiguchi, M. (1992) *Nature 355*, 273−275.
9. Shibutani, S., Takeshita, M., and Grollman, A. P. (1991) *Nature 349*, 431−434.
10. Cheng, K. C., Cahill, D. S., Kasai, H., Nishimura, S., and Loeb, L. A. (1992) *J. Biol. Chem. 267*, 166−172.
11. Treffers, H. P., Spinelli, V., and Belser, N. O. (1954) *Proc. Natl. Acad. Sci. U.S.A. 40*, 1064−1071.
12. Yanofsky, C., Cox, E. C., and Horn, V. (1966) *Proc. Natl. Acad. Sci. U.S.A. 55*, 274−281.
13. Tsuzuki, T., Egashira, A., Igarashi, H., Iwakuma, T., Nakatsuru, Y., Tominaga, Y., Kawate, H., Nakao, K., Nakamura, K., Ide, F., Kura, S., Nakabeppu, Y., Katsuki, M., Ishikawa, T., and Sekiguchi, M. (2001) *Proc. Natl. Acad. Sci. U.S.A. 98*, 11456−11461.
14. Tassotto, M. L., and Mathews, C. K. (2002) *J. Biol. Chem.* 277, 15807−15812.

15. Abeygunawardana, C., Weber, D. J., Gittis, A. G., Frick, D. N., Lin, J., Miller, A.-F., Bessman, M. J., and Mildvan, A. S. (1995) *Biochemistry 34*, 14997−15005.
16. Massiah, M. A., Saraswat, V., and Mildvan, A. S. (2002) Abstract 43rd ENC meeting, Asilomar, CA, April 14−19, 2002, Abstract no. W/T P-198, p 263.
17. Abeygunawardana, C., Weber, D. J., Frick, D. N., Bessman, M. J., and Mildvan, A. S. (1993) *Biochemistry 32*, 13071−13080.
18. Rückert, M., and Otting, G. (2000) *J. Am. Chem. Soc. 122*, 7793−7797.
19. Ottiger, M., Delaglio, F., and Bax, A. (1998) *J. Magn. Reson. 131*, 373−378.
20. Delaglio, F., Grzesiek, S., Vuister, G. W., Zhu, G., Pfeifer, J., and Bax, A. (1995) *J. Biomol. NMR 6*, 277−93.
21. Johnson, B. A., and Blevins, R. A. (1994) *J. Biomol. NMR 4*, 603−614.
22. Lee, W., Revington, M., Arrowsmith, C., and Kay, L. E. (1994) *FEBS Lett. 350*, 87−90.
23. Massiah, M. A., Abeygunawardana, C., Gittis, A. G., and Mildvan, A. S. (1998) *Biochemistry 37*, 14701−14712.
24. Cornilescu, G., Delaglio, F., and Bax, A. (1999) *J. Biomol. NMR 13*, 289−302.
25. Stein, E. G., Rice, L. M., and Brunger, A. T. (1997) *J. Magn. Reson. 124*, 154−164.
26. Brunger, A. T., Adams, P. D., Clore, G. M., Delano, W. L., Gros, P., Grosse-Kunstleve, R. W., Jiang, J.-S., Kuszewski, J., Nilges, M., Pannu, N. S., Read, R. J., Rice, L. M., Simonson, T., and Warren, G. L. (1998) *Acta Crystallogr. D54*, 905−921.
27. Frick, D. N., Weber, D. J., Abeygunawardana, C., Gittis, A. G., Bessman, M. J., and Mildvan, A. S. (1995) *Biochemistry 34*, 5577−5586.
28. Tolman, J. R., Flanagan, J. M., Kennedy, M. A., and Prestegard, J. H. (1995) *Proc. Natl. Acad. Sci. U.S.A. 92*, 9279−9283
29. Tjandra, N., and Bax, A. (1997) *Science 278*, 1111−1114.
30. Clore, G. M., Gronenborn, A. M., and Bax, A. (1998) *J. Magn. Reson. 133*, 216−221.
31. Clore, G. M., Gronenborn, A. M., and Tjandra, N. (1998) *J. Magn. Reson. 131*, 159−162.
32. Bai, Y., Milne, J. S., Mayne, L., and Englander, S. W. (1993) *Proteins: Struct., Funct., Genet. 17*, 75−86.
33. Wüthrich, K. (1986) *NMR of Proteins and Nucleic Acids*, pp 123−125, John Wiley and Sons, New York.
34. Weber, D. J., Abeygunawardana, C., Bessman, M. J., and Mildvan, A. S. (1993) *Biochemistry 32*, 13081−13088.
35. Lin, J., Abeygunawardana, C., Frick, D. N., Bessman, M. J., and Mildvan, A. S. (1996) *Biochemistry 35*, 6715−6726.
36. Laskowski, R. A., MacArthur, M. W., Moss, D. S., and Thornton, J. M. (1993) *J. Appl. Crystallogr. 26*, 283−291.
37. Conyers, G. B., Wu, G., Bessman, M. J., and Mildvan, A. S. (2000) *Biochemistry 39*, 2347−2354.
38. Fletcher, J. I., Swarbrick, J. D., Maksel, D., Gayler, K. R., and Gooley, P. R. (2002) *Structure 10*, 205−213.
39. Graham, D. L., Lowe, P. N., Grime, G. W., Marsh, M., Rittinger, K., Smerdon, S. J., Gamblin, S. J., and Eccleston, J. F. (2002) *Chem. Biol. 9*, 375−381.
40. Sanner, M. F., Olson, A. J., and Spencer, J. C. (1995) *Proceedings of Eleventh Association for Computational Machinery Symposium on Computational Geometry*, A. C. M. Press, New York, pages C6−C7.
41. Wang, C., Pawley, N. H., and Nicholson, L. K. (2001) *J. Mol. Biol. 313*, 873−877.
42. Kraulis, P. J. (1991) *J. Appl. Crystallogr. 24*, 946−950.

BI030105P